


Characterization of unconventional hydrogen flame propagation in narrow gaps

Jorge Yáñez Escanciano* and Mike Kuznetsov 

Institute for Thermal Energy Technology and Safety, Karlsruhe Institute of Technology, 76131 Karlsruhe, Germany

Fernando Veiga-López 

Departamento de Ingeniería Térmica y de Fluidos, de la Universidad Carlos III de Madrid, 28911, Leganés, Madrid, España



(Received 25 September 2020; accepted 9 February 2021; published 3 March 2021)

The physical limits of the unconventional flame propagation regimes recently discovered [Veiga-Lopez *et al.*, *Phys. Rev. Lett.* **124**, 174501 (2020)] are analyzed. These regimes appear in combustible gaseous mixtures approaching the lean quenching limit of hydrogen-air flames in narrow gaps. They are characterized by a split of the flame front into a dendritic and a bifurcating set of flame cells separated by nonburned material. A feature selection analysis utilizing dimensionless numbers is applied to reveal the most significant parameters governing the separation between unconventional and traditional flame propagation regimes. It is concluded that (a) the outbreak of unconventional propagation is mostly due to heat losses, (b) the phenomenon is governed by the Peclet number and only appears in thin channels, and (c) the Lewis number does not determine the propagation regime. Additionally, an equation describing the optimal border of the unconventional regime is derived from experiments.

DOI: [10.1103/PhysRevE.103.033101](https://doi.org/10.1103/PhysRevE.103.033101)

I. INTRODUCTION

Propagation of flames in confined environments have been the object of numerous research [1–5]. In most of the works devoted to tubes or confined flame propagation, the main goal was to investigate the flame instability, its acceleration, and/or Deflagration to Detonation Transition (DDT) transition far from the flammability limits. Here we want to focus our study on the flame behavior approaching the lower flammability limit, in a situation similar to the studies made by Maruta *et al.* [6], who analyzed the flame propagation in narrow channels in the presence of heat losses.

In particular, the lower flammability limit of hydrogen-air mixtures at unconfined ambient conditions is equal to 4% mol. of H₂. Nevertheless, if the combustion takes place in a confined space, then the flame may extinguish for very reactive mixtures at much higher hydrogen concentration.

To systematically analyze the divergence between confined and unconfined environments, the flame propagation regimes for different hydrogen-air mixtures in a narrow gap were investigated in Ref. [7]. In an enclosure, combustion propagation is governed by the thickness of the gap and by the mixture reactivity. In their analysis, the authors use Peclet number as dimensionless scale factor (the gap size normalized by the laminar flame thickness as a measure of chemical reactivity).

The expected results were obtained until the quenching limit was reached. An anomaly was observed beyond the traditional quenching limit $Pe = 42$ [8]. Within the interval $9 < Pe < 42$, where the laminar flame thickness is comparable to the size of the enclosure, a variety of unprecedented

flame propagation regimes were presented in Ref. [9]. In particular, these newly discovered regimes are characterized by a division of the expected continuous flame front into a set of tiny flame cells separated by a mass of nonburned material.

Four categories of such flame propagation regimes were reported depending on the conditions of the experiment (Fig. 1):

(a) Monocellular, in which the so-called *one-headed finger* category is obtained.

(b) *One-headed branching*, where a singular monocellular front may bifurcate cyclically into several independent monocellular fronts producing menorah-like structures.

(c) Bicellular, a class that received the name *two-headed finger*.

(d) *Two-headed branching*, where two-headed fronts also bifurcate cyclically producing palm treelike structures.

Furthermore, the results of the experiments in Ref. [9] showed two familiar categories: (e) no-ignition and (f) conventional continuous flame front propagation (Fig. 2), which are also considered here.

Figure 3 represents the diagram of state for hydrogen flame propagation in narrow gaps in terms of gap size versus hydrogen concentration. The diagram depicts the experimental results obtained but does not provide an explanation of the nature of the process.

Given the available literature, mass diffusivity, heat losses, and gravity appear to be the significant factors capable of creating dendritic combustion structures.

(i) Mass diffusivity

The deficit of hydrogen at lean concentrations might be compensated for strong diffusion from surrounding material creating a localized isolated area of richer, and thus hotter, combustion. This would counteract heat losses, keeping the

*jorge.yanez@kit.edu

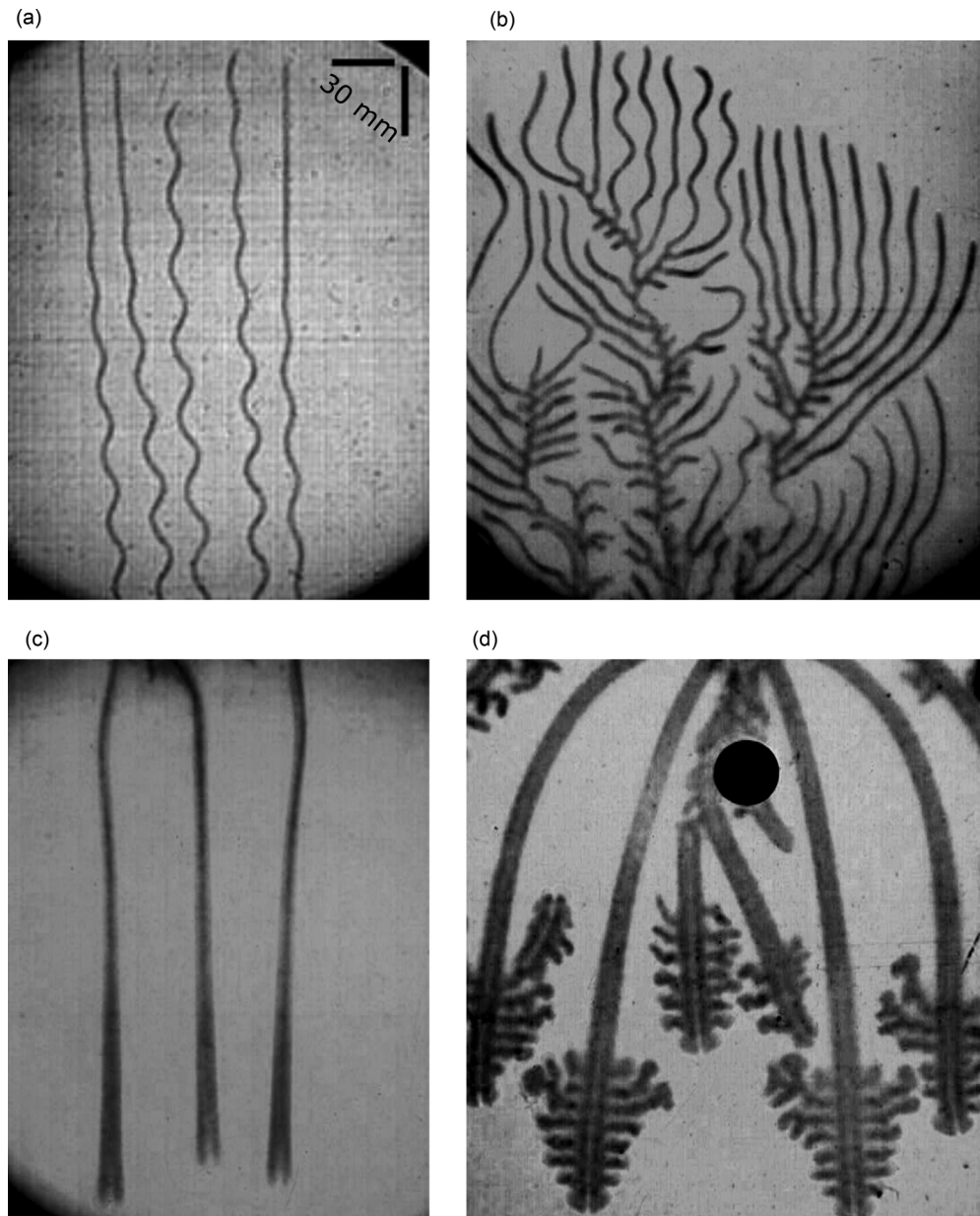


FIG. 1. Unconventional flame propagation categories: (a) one-headed finger, (b) one-headed branching, (c) two-headed fingers, and (d) two-headed branching.

local gas above the limiting temperature and, therefore, sustaining the combustion process at these spots.

This mechanism was recognized in Ref. [9] as one of the governing issues in their experiments. In their analysis, they even related the width of the unburned material in between branches to the depletion of fuel.

In Refs. [10–12], dendritic combustion patterns were observed on smoldering in Hele-Shaw cells. These authors also associated the existence of the phenomena to the mass diffusivity of the deficient component.

In a theoretical study [13], the existence of fragmented flame structures as a phenomenon caused by the diffusivity was explained. They were even able to describe these fragmented fronts despite considering adiabatic conditions for thermodiffusive unstable flames.

(ii) Heat losses

In addition to these findings, it also appears that heat losses can generate a similar combustion pattern.

In Ref. [14] it was stated that fragmented reaction areas appear separated by quenched parts as a product of heat losses.

The phenomenon was also numerically investigated in Ref. [15] with highly diffusive flames. It was interpreted that the existence of similar flame propagation regimes is a function of conductive heat losses. Notably, the authors of the study concluded that the intensity of the heat losses to the sidewalls determine the two- or single-headed propagation regime.

Results shown in Ref. [9] also relate the existence of nonconventional propagation regimes to the heat losses, in agreement with the findings in Ref. [7]. Both studies consider the Peclet number to be a key parameter to understanding the results.



FIG. 2. Conventional continuous flame front structure.

(iii) Gravity

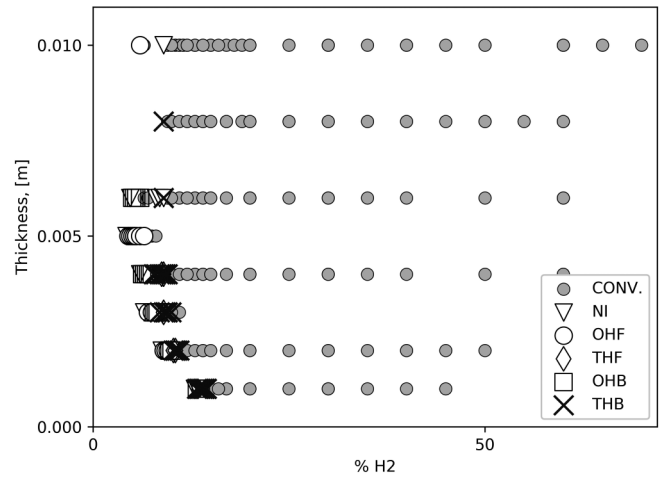
The test apparatus is positioned vertically, so gravity could be a significant factor. This is due to the strong influence of buoyancy on flame propagation limits for up- and downward propagating hydrogen flames.

Despite the previous interpretations, an exhaustive exploitation of the significant amount of experimental data obtained in Ref. [9] is still incomplete. In this study, we carry out its statistical analysis. We seek to clarify the most important of the questions related to the newly observed phenomena, that is, What are the conditions determining conventional or unconventional propagation regimes?

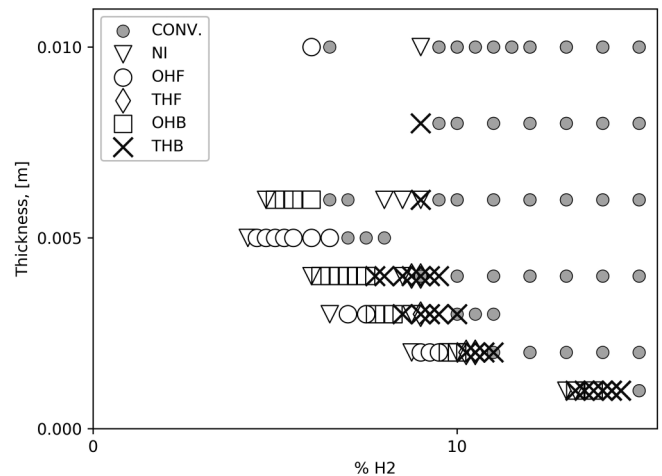
We perform our study with machine learning techniques. Machine learning [16] is a branch of computational statistics [17] sets of data are analyzed systematically with the goal of extracting information. Due to the fast development of this branch in the past several years, large numerical libraries like Scikit-Learn [18] have become publicly available. We will utilize *feature selection* techniques [19] to systematically extract the most significant parameters that determine the defining conditions.

II. ANALYSIS

The strategy used in this study is as follows.



(a)



(b)

FIG. 3. Experimental matrix. (a) Full matrix. (b) Lean experiments. Different phenomena registered: conventional combustion mode (CONV), no-ignition (NI), one-headed finger (OHF), two-headed fingers (THF), one-headed branching (OHB), and two-headed branching (THB).

A. Preprocessing

The number of experiments available for each of the six categories described in the introduction do not allow for significant segregation of each of the propagation regimes. Therefore, we agglomerate all *unconventional* categories to find the optimal border between conventional (Fig. 2) and unconventional (Fig. 1) modes. Among all the tests, downward-propagating tests only will be considered in our study, captured in Fig. 4. Note that we exclude upward propagation experiments because there is not a large-enough sample size for a confident analysis.

B. Features

From the layer thickness and properties of the mixture, we shall generate dimensionless numbers to provide a physical interpretation of the experimental results. They

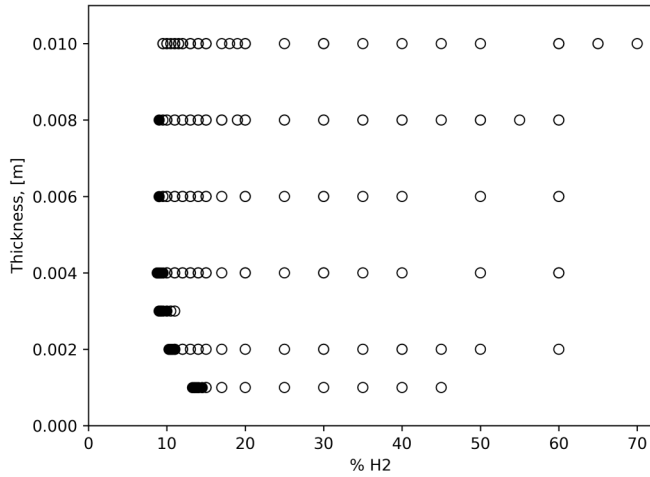


FIG. 4. Dicotomic experimental matrix. White and black points represent conventional and unconventional propagation, respectively.

are as follows: Reynolds number, $Re = LS_L$; Peclet number, $Pe = L/\delta_T$; Prandtl number, $Pr = \nu/\chi$; Richardson number, $Ri = g\beta(T_b - T_0)L/S_L^2$; Rayleigh number, $Ra = g\beta(T_b - T_0)L^3/(\chi\nu)$; Schmidt number, $Sc = \nu/D$; Lewis number, $Le = \chi/D$; Zeldovich number, $Ze = E(T_b - T_0)/RT_b^2$; expansion rate $\sigma_1 = \rho_0/\rho_b$; modified expansion rate $\sigma_2 = \rho_{cold\ products}/\rho_0$; and Froude number $Fr = S_L/\sqrt{gL}$. These numbers depend on the basic magnitudes of the gaseous mixture and the flame, such as the laminar flame speed S_L , adiabatic combustion temperature T_b , an overall activation energy E , kinematic viscosity ν , thermal diffusivity χ , molecular diffusion D , integral scale of the system or gap size L , gravitational acceleration g , and thermal expansion of the gas β .

The aforementioned dimensionless numbers characterize the process with respect to viscosity (Re, Pr), diffusion (Le, Sc), buoyancy (Ri, Ra, Fr), and chemical reactivity (Re, Pe, Ze).

C. Nusselt number

Heat losses have been identified as one of the main parameters of the problem.

(i) Bergman correlation

The usage of the Nusselt number for laminar flow along a flat plate, as described in [20],

$$Nu = 0.33Re_x^{1/2}Pr^{1/3}, \quad (1)$$

poses two problems. First, the distance, x , parallel to the plate is one of its main dependencies. In our case, this distance is measured from the flame position. This value is ill defined due to the multiplicity of fronts.

Second, Re_x also depends on the flame propagation velocity, S , and not on S_L . In the study [9], it was impossible to the velocity of the propagating flame from their experiments, thus the real flame velocity S remains unknown.

To circumvent these shortcomings, we take into account the minimal distance capable of cooling the whole thickness, h , of the gas gap, $h/2 = \sqrt{\nu x/S}$. Also, we will utilize the laminar

burning velocity, S_L . Substituting, we obtain

$$Nu_1 \approx 0.033RePr^{1/3}. \quad (2)$$

(ii) Kuznetsov correlation

The estimation of the Nusselt number according to Eq. (1) is questionable under these particular conditions. This is due to the presence of heat losses caused by steam condensation [7]. The effect of condensation was shown to be very significant in Refs. [7,9]. The presence of water fog or even droplets on the internal side of the Plexiglas plates confirm this fact. Therefore, the empirical correlation for the Nusselt number considering condensation due to [21] was also utilized:

$$Nu_2 = 10.3Re^{0.3}. \quad (3)$$

D. B parameter

In the numerical calculations dedicated to *unconventional* propagation [15,22], the dimensionless parameter B was also considered:

$$B = \frac{k_w/h_w}{k_g/h}, \quad (4)$$

where k_w and k_g are the conductivity of the wall and the gas and h_w and h are their respective thicknesses. The ratio $(k_w h)/(k_g h_w)$ describes the conductive heat transfer in the wall compared to that of the gaseous gap per Kelvin. It extends the classical formulation of [23,24] and is very similar to the parameter used in Ref. [25].

E. Additional parameters

Two additional dimensionless parameters can also be introduced into the analysis. First, we have the Biot number,

$$Bi = \frac{\alpha h_w}{k_w}, \quad (5)$$

where α is the thermal conductivity at the interface. We extract α from Nu, which yields

$$Bi_i = \frac{h_w \chi}{k_w h} Nu_i, \quad (6)$$

and thus gives two Bi numbers for their respective Nu.

Next we have the Fourier number,

$$Fo = \frac{\chi t}{L^2}, \quad (7)$$

where t is the characteristic time to reach a certain temperature, which results in

$$Fo = Pe^{-2}, \quad (8)$$

and therefore can be disregarded.

F. Limitations

Some magnitudes defined above, like Re, were characterized considering S_L and not the velocity measured in the study S . Similar shortcomings also exists for T_b , which is clearly different than the temperature reached in between the two plates. These shortcomings could be possible source of insignificance or inaccuracy.

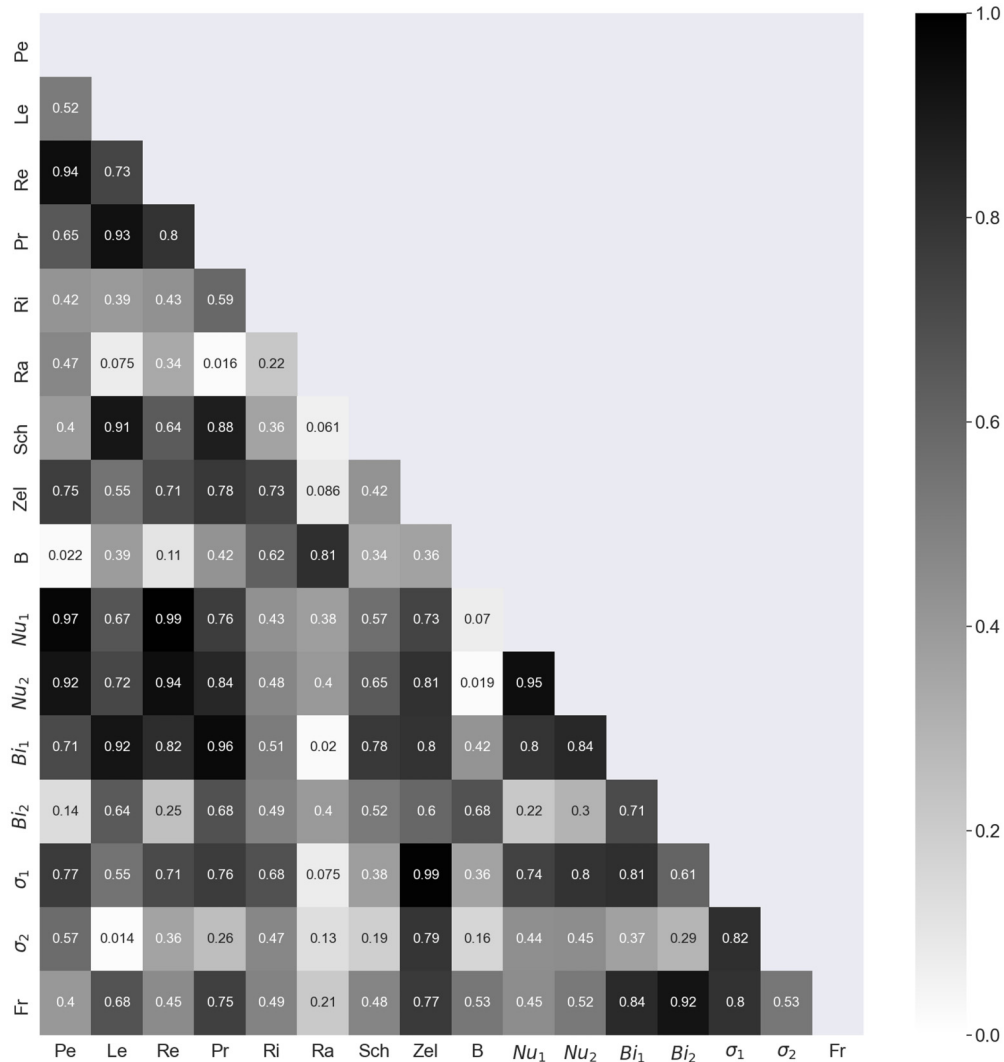


FIG. 5. Autocovariance matrix.

G. Recapitulation

In summary, each experiment can be characterized by the following vector:

$$(Re, Pe, Pr, Ri, Ra, Sc, Le, Ze, B, Nu_1, Nu_2, Bi_1, Bi_2, \sigma_1, \sigma_2, Fr). \tag{9}$$

Note that the addition of more parameters would increase the reliability of the conclusions.

H. Reduction of dimensionality

We may reduce the dimension of the previous vector by disregarding highly correlated components. We can study the correlation of the different variables by calculating the autocovariance matrix [26], plotted in Fig. 5. In this figure, we can see the correlation of the variables to each other. Higher values in each cell means a higher degree of correlation between elements of the matrix.

We disregard variables correlated to others more than a predetermined threshold, which was set at 0.9. Given that assumption, this set of numbers appear to be correlated. On

one side, we have Re, Pe, and Nu, and on the other Pr, Le, Sc, Bi₁, and Le. It is indifferent which of those numbers we keep as they statistically contain the same information. To be more coherent with referenced literature, we will use

$$(Pe, Ri, Ra, Le, Ze, B, Bi_2, \sigma_2). \tag{10}$$

I. Segregation

We separate the experiments shown in the dichotomic matrix (Fig. 4) using a linear correlation in the logarithmic space generated by a pair of variables. Later, we identify the optimal number of parameters that may govern the phenomena. Additionally, we seek to clarify which pair better correlates the experimental findings. Please note that we disregard all nonlinear borders that could provide even better separation between the unconventional and the conventional regions, making it easier to physically understand our results.

III. FEATURE SELECTION

Recursive feature elimination is a technique that allows selecting features by recursively considering smaller and

TABLE I. Results of recursive feature elimination with cross-validation.

Number of variables	Score
1	0.89
2	0.90
3	0.90
4	0.89
5	0.89
6	0.89
7	0.89
8	0.89

smaller sets of variables [27]. In our study, we will utilize a further development of this technique that includes a *cross-validation* step [28]. This implies the division of the whole data into subsets. The importance of each feature will then be analyzed in each subset, modeling and evaluating with regard to its complementary. This technique is called *recursive feature elimination with cross-validation* (RFECV), and it is available in Scikit-Learn. RFECV requires the user to provide a classification model that provides a score for each feature and, therefore, a way to assess its importance.

Support vector classification (SVC) is a method inside of *support vector machines* (SVM) methodologies [29,30] that provides the required classification. Succinctly, SVM provides a classification for data belonging to dichotomic classes by separating them with an optimal hyperplane. The hyperplane is chosen so that the distance from it to the nearest data point in each dichotomic category is maximized. By ranking which feature provides a cleaner separation, we can score each of the variables.

The result of this methodology applied to our data is contained in Tables I and II.

In Table I, we observe that the best separation is achieved with two variables. We also conclude that three or more variables provide a similar quality of separation. Likewise, the separation based in one variable is also similar than the one achieved with three or more.

In Table II we depict the relative importance of each of the variables. The most significant variables are Pe and Ri followed by the Rayleigh number. The diffusion factor Le, σ_2 , and the chemical reactivity factor, Ze, are less significant. Thus, the optimal SVM model should be the function and

TABLE II. Importance ranking by recursive feature elimination results.

Variable	Importance
Pe	1
Le	6
Ri	1
Ra	2
Ze	5
B	4
Bi ₂	3
σ_2	7

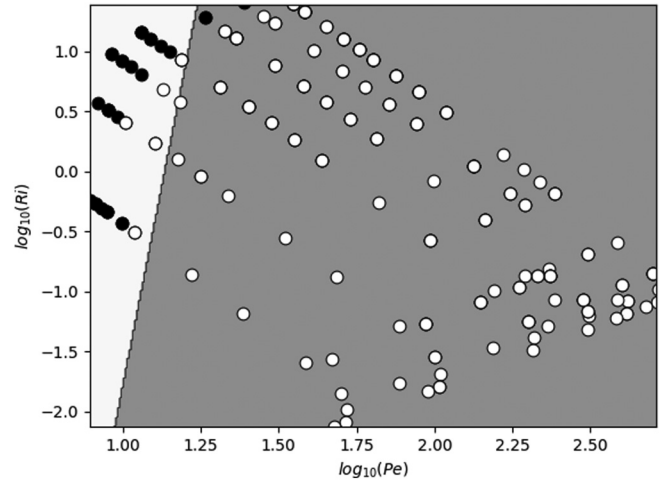


FIG. 6. SVM model based on Pe and Ri. Optimal model. White points: Conventional propagation. Black points: Unconventional propagation. White region: SVM model unconventional propagation prediction. Gray region: SVM model conventional propagation prediction.

the argument of the most significant variables Pe and Ri (see Fig. 6).

From the SVM model, the optimal border in Fig. 6 is

$$\log_{10}(\text{Ri}) \approx 13.2 \log_{10}(\text{Pe}) - 15.0, \tag{11}$$

or

$$\text{Ri} \approx \frac{\text{Pe}^{13.2}}{10^{15.0}}. \tag{12}$$

The importance of Pe is shown by its power. Pe is collinear with Re and Nu, so that Pe represents the statistical importance of the thickness of the tube, the flow regime, and the heat losses. Ri shows the mild importance of gravity and shear. This is also in agreement with the findings of Table I where separation based on a single variable obtained a surprisingly good score.

IV. SUBOPTIMAL BORDERS

In this section, we explore the experimental data as a function of other variables. This may allow for an alternative interpretation of the results.

A. Secondary importance variables

We reconsider the relative importance of the variables represented in Table II. We may enlarge our assessments by including the next more significant variable, Ra, and represent (Pe, Ra) and (Ri, Ra). This has been done in Figs. 7 and 8.

The separation of the data achieved by the usage of the pair Pe, Ra is relatively good. The implicit model implies that unconventional propagation is reached if $\text{Ra} \gtrsim 10^{51} \text{Pe}^{-42}$, that is, if Ra is much less important than Pe. The expression means that the separation line versus Pe is almost vertical and simplifies the critical condition to

$$\text{Pe} \lesssim 15, \tag{13}$$

for unconventional propagation.

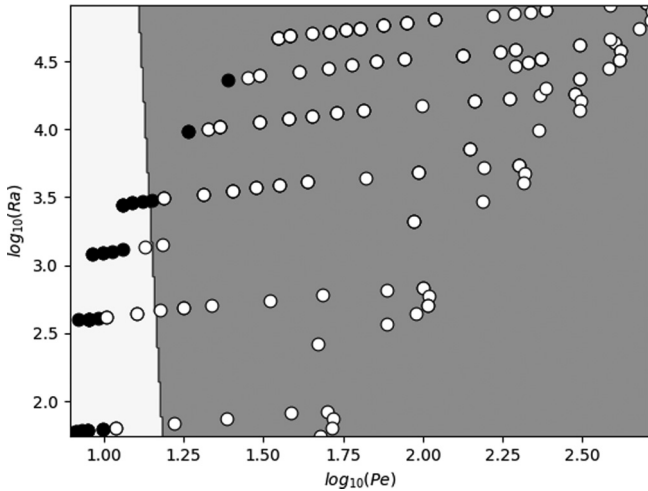


FIG. 7. SVM model using Pe, Ra. For the points and regions meaning, see Fig. 6.

We represent now the other secondary pair (Ri, Ra). From the modeling obtained, we derive a border,

$$Ra \gtrsim 251Ri^{1.1}. \tag{14}$$

We recall here the physical meaning of Ri and Ra. The relative importance of buoyancy to shear in a flow is Ri. The importance of heat convection compared to conduction is Ra. Purely convective heat transfer is represented as $Ra > 1000$. Purely conductive heat transfer is $Ra < 10$. Between these two values, both heat transfer mechanisms are combined. Most of the points in Fig. 8 lay above $Ra > 1000$. The border found shows the relative importance of buoyancy or shear and convection. The power of Ra and Ri shows that the flow regime and the heat transfer have a similar importance close to 1.

B. Separate ranking of the variables

We continue exploring the experimental results. Next, we will rank the importance of each of the significant dimension-

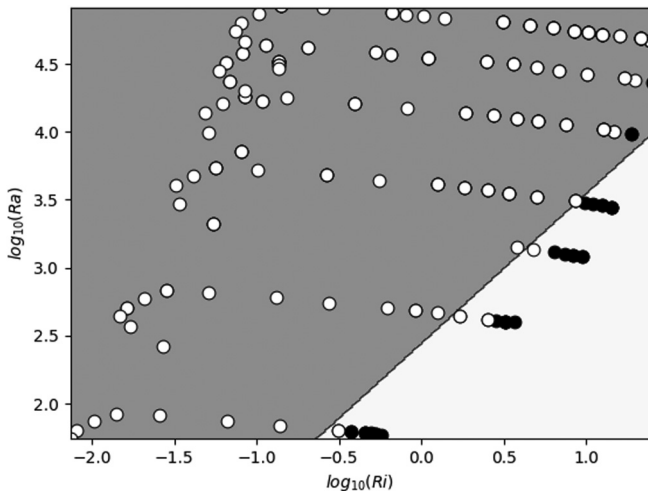


FIG. 8. SVM model using Ri and Ra. For the points and regions meaning, see Fig. 6.

TABLE III. Ranking individual variables.

Number	<i>F</i> value	Mutual information
Pe	129.3	0.29
Le	13.1	0.08
Ri	9.5	0.16
Ra	71.9	0.25
Ze	33.2	0.24
<i>B</i>	25.9	0.27
Bi ₂	0.02	0.14
σ ₂	14.2	0.23

less numbers by a second procedure, this time not combined but individually separated. This ranking can be done by the ANOVA *F* value [31] and the mutual information classification [32] methods. Conveniently, both are readily available in Scikit.

The results obtained are included in Table III. Pe and Ra appear to be the most significant variables with the largest *F* value. Pe and *B* are the most significant variables utilizing mutual information. The Lewis number, Le, and the Biot number, Bi₂, have the lowest significance.

Therefore, we may study the separation between conventional and unconventional flame propagation considering the pair Pe and *B*. This is shown in Fig. 9. The separation model was again generated utilizing SVM methodology.

The separation line in Fig. 9 shows that unconventional propagation is reached for $B \gtrsim 10^{38}Pe^{-38}$. This transforms again into $Pe \lesssim 15$, underlining the enhanced importance of Pe compared with *B*.

At this stage, the authors want to underline a caveat clearly visible in Figs. 6–9. We have been utilizing straight lines to represent the optimal borders in the diagrams in spite of the significant curvature visible in the boundary between the regimes. In our opinion, an interpretation of the curvature of the data could be achieved considering the border as the maximum, or minimum, between two lines. This kind of interpretation is typical of logarithmic representation. This

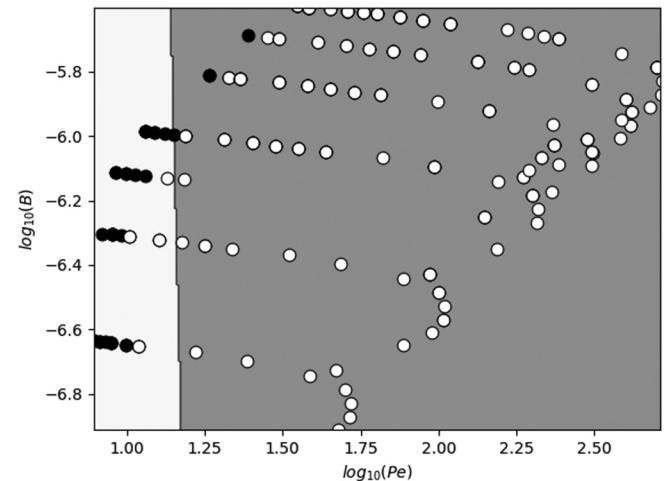


FIG. 9. SVM model using Pe, *B*. Points and regions meaning, see Fig. 6.

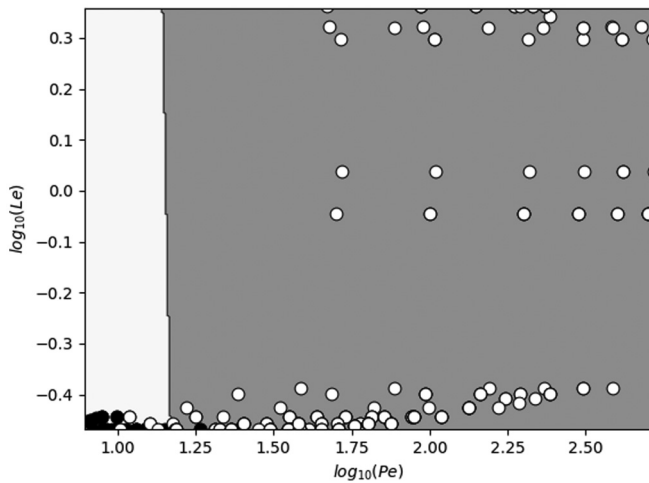


FIG. 10. SVM model using Pe and Le . For the points and regions meaning, see Fig. 6.

apparent min-max behavior may be achieved as the sum of two terms which prevails in different zones. Also, this may be consistent with data obtained in two different regimes for Ra larger and smaller than 1000 and Ri larger and smaller than 1. Nevertheless, this interpretation is speculative. Also, the limited number of points have prevented the further exploration of this technique.

C. Lack of significance of Le

The results shown in Refs. [10–12] support that diffusivity determines the distance of unburned pockets between the flame fingers. The diffusivity should counteract heat losses in Hele-Shaw cells making the flame hotter by the diffusion transport of deficient components towards the reaction zone [10,11,33].

On the contrary, our SVM analysis shows that Le has no importance in determining the flame regime (Fig. 10). Several reasons support this finding:

(i) The range of concentrations of interest is from 4 to 15 vol.% H_2 . In this range, the flame structure changes dramatically. Nevertheless, the Lewis number only changes slightly from 0.31 to 0.34. However, the heat losses change dramatically, completely modifying the combustion process and the flame structure.

(ii) The size of the gap does not influence the diffusion process. To be significant, a Knudsen number of order of one is required. This corresponds to much narrower channels, down to the size of 1 micrometer.

(iii) Independent of small Lewis number ($Le \ll 1$) for all mixtures tested, the size of the narrow gap decreases or suppresses the thermodiffusive instability. This is due to the critical Peclet number for thermodiffusion instability which is $Pe_c = 50\text{--}150$ ([34–36]). This is larger than the typical Pe for the unusual flame propagation, $Pe = 15$. This fact reduces the significance of Le for the threshold evaluation.

V. CONCLUSIONS

In conclusion, unconventional propagation happens in thin tubes in which heat losses are significant, in agreement with the idea exposed in Ref. [9]. Equation (11) provides an empirical correlation of the limits of the propagation regime.

The present study excludes Le as a significant parameter to determine the phenomena of unconventional propagation. Despite this, unconventional propagation regimes only occur, as reported, exclusively for $Le \ll 1$.

Unconventional propagation is mainly determined by Pe , that is, by the heat losses dictated by the thickness of the channel.

-
- [1] V. Bychkov, V. Akkerman, G. Fru, A. Petchenko, and L.-E. Eriksson, Flame acceleration in the early stages of burning in tubes, *Combust. Flame* **150**, 263 (2007).
 - [2] D. Valiev, V. Bychkov, V. Akkerman, C. K. Law, and L.-E. Eriksson, Flame acceleration in channels with obstacles in the deflagration-to-detonation transition, *Combust. Flame* **157**, 1012 (2010).
 - [3] M. Liberman, G. Sivashinsky, D. Valiev, and L.-E. Eriksson, Numerical simulation of deflagration-to-detonation transition: The role of hydrodynamic instability, *Intl. J. Transp. Phenom.* **8**, 253 (2006).
 - [4] V. N. Gamezo, T. Ogawa, and E. S. Oran, Numerical simulations of flame propagation and ddt in obstructed channels filled with hydrogen–air mixture, *Proc. Combust. Inst.* **31**, 2463 (2007).
 - [5] B. Demirgok, O. Ugarte, D. Valiev, and V. Akkerman, Effect of thermal expansion on flame propagation in channels with nonslip walls, *Proc. Combust. Inst.* **35**, 929 (2015).
 - [6] K. Maruta, T. Kataoka, N. I. Kim, S. Minaev, and R. Fursenko, Characteristics of combustion in a narrow channel with a temperature gradient, *Proc. Combust. Inst.* **30**, 2429 (2005).
 - [7] M. Kuznetsov and J. Grune, Experiments on combustion regimes for hydrogen/air mixtures in a thin layer geometry, *Int. J. Hydrogen Energy* **44**, 8727 (2019).
 - [8] J. Jarosinski, J. Podfilipski, and T. Fodemski, Properties of flames propagating in propane-air mixtures near flammability and quenching limits, *Combust. Sci. Technol.* **174**, 167 (2002).
 - [9] F. Veiga-López, M. Kuznetsov, D. Martínez-Ruiz, E. Fernández-Tarrazo, J. Grune, and M. Sánchez-Sanz, Unexpected Propagation of Ultra-Lean Hydrogen Flames in Narrow Gaps, *Phys. Rev. Lett.* **124**, 174501 (2020).
 - [10] O. Zik, Z. Olami, and E. Moses, Fingering Instability in Combustion, *Phys. Rev. Lett.* **81**, 3868 (1998).
 - [11] O. Zik and E. Moses, Fingering instability in combustion: An extended view, *Phys. Rev. E* **60**, 518 (1999).

- [12] S. Olson, F. Miller, S. Jahangirian, and I. Wichman, Flame spread over thin fuels in actual and simulated microgravity conditions, *Combust. Flame* **156**, 1214 (2009).
- [13] L. Kagan and G. Sivashinsky, Pattern formation in flame spread over thin solid fuels, *Combust. Theor. Model.* **12**, 269 (2008).
- [14] L. Kagan and G. Sivashinsky, Self-fragmentation of nonadiabatic cellular flames, *Combust. Flame* **108**, 220 (1997).
- [15] D. Martínez-Ruiz, F. Veiga-López, D. Fernández-Galisteo, V. N. Kurdyumov, and M. Sánchez-Sanz, The role of conductive heat losses on the formation of isolated flame cells in hele-shaw chambers, *Combust. Flame* **209**, 187 (2019).
- [16] T. M. Mitchell, *Machine Learning* (McGraw-Hill, New York, 1997), p. 414.
- [17] J. F. Monahan, *Numerical Methods of Statistics* (Cambridge University Press, Cambridge, UK, 2011).
- [18] F. Pedregosa, G. Varoquaux, A. Gramfort, V. Michel, B. Thirion, O. Grisel, M. Blondel, P. Prettenhofer, R. Weiss, V. Dubourg, J. Vanderplas, A. Passos, D. Cournapeau, M. Brucher, M. Perrot, and E. Duchesnay, Scikit-learn: Machine learning in Python, *J. Mach. Learn. Res.* **12**, 2825 (2011).
- [19] I. Guyon and A. Elisseeff, An introduction to variable and feature selection, *J. Mach. Learn. Res.* **3**, 1157 (2003).
- [20] T. L. Bergman, F. P. Incropera, D. P. DeWitt, and A. S. Lavine, *Fundamentals of Heat and Mass Transfer* (John Wiley & Sons, New York, 2011).
- [21] M. Kuznetsov, I. Matsukov, and S. Dorofeev, Heat loss rates from hydrogen-air turbulent flames in tubes, *Combust. Sci. Technol.* **174**, 75 (2002).
- [22] F. Veiga-López, Flame propagation in narrow channels, Ph.D. thesis, Universidad Carlos III, Madrid, Spain (2020).
- [23] V. N. Kurdyumov and M. Matalon, Flame acceleration in long narrow open channels, *Proc. Combust. Inst.* **34**, 865 (2013).
- [24] V. N. Kurdyumov and M. Matalon, Self-accelerating flames in long narrow open channels, *Proc. Combust. Inst.* **35**, 921 (2015).
- [25] C. Jimenez and V. N. Kurdyumov, Propagation of symmetric and non-symmetric lean hydrogen-air flames in narrow channels: Influence of heat losses, *Proc. Combust. Inst.* **36**, 1559 (2017).
- [26] W. Feller, *An Introduction to Probability Theory and Its Applications* (John Wiley & Sons, New York, 1971).
- [27] I. Guyon, S. Gunn, M. Nikravesh, and L. A. Zadeh, *Feature Extraction: Foundations and Applications*, Vol. 207 (Springer, Berlin, 2008).
- [28] M. Kuhn and K. Johnson, *Feature Engineering and Selection: A Practical Approach for Predictive Models* (CRC Press, Boca Raton, FL, 2019).
- [29] C.-C. Chang and C.-J. Lin, Libsvm: A library for support vector machines, *ACM Trans. Intell. Syst. Technol.* **2**, 1 (2011).
- [30] L. Wang, *Support Vector Machines: Theory and Applications*, Vol. 177 (Springer Science & Business Media, New York, 2005).
- [31] D. R. Cox, *Principles of Statistical Inference* (Cambridge University Press, Cambridge, UK, 2006).
- [32] T. Cover and J. Thomas, *Elements of Information Theory* (Wiley Online Library, Hoboken, New Jersey, 1991).
- [33] E. Fernández-Tarrazo, A. L. Sánchez, A. Liñán, and F. A. Williams, Flammability conditions for ultra-lean hydrogen pre-mixed combustion based on flame-ball analyses, *Int. J. Hydr. Energy* **37**, 1813 (2012).
- [34] S. Yang, A. Saha, F. Wu, and C. K. Law, Morphology and self-acceleration of expanding laminar flames with flame-front cellular instabilities, *Combust. Flame* **171**, 112 (2016).
- [35] J. Yanez and M. Kuznetsov, An analysis of flame instabilities for hydrogen-air mixtures based on Sivashinsky equation, *Phys. Lett. A* **380**, 2549 (2016).
- [36] J. Yaguchi, W. Kim, T. Mogi, and R. Dobashi, Flame acceleration and blast wave of $H_2-O_2-N_2-Ar$ mixtures in unconfined areas, (unpublished).